ATLAS NOTE

ATLAS-CONF-2016-094

30th August 2016

Search for new phenomena in a lepton plus high jet multiplicity final state with the ATLAS experiment using $\sqrt{s}$ = 13 TeV proton-proton collision data

The ATLAS Collaboration

Abstract

A search for new phenomena in final states characterized by high jet multiplicity, an isolated lepton (electron or muon) and either zero or at least three b-tagged jets is presented. The search uses 14.8 fb^{-1}of $\sqrt{s}$ = 13 TeV proton-proton collision data collected by the ATLAS experiment at the Large Hadron Collider in 2015 and 2016. The background is estimated by extrapolating a template of the b-tagged jet multiplicity, obtained at medium jet multiplicity, to the higher jet multiplicities used in the search. No significant excess of events is observed over the background expectation and 95% confidence level limits are extracted constraining supersymmetric models where the gluino is pair-produced, and decays to a pair of top quarks and jets through the R-parity violating decay of either the neutralino into three quarks or the top squark into a b- and an s- quark. In addition model-independent limits are set on the contribution of new phenomena to the signal region yields of up to 8 fb at 95% confidence level.

ATLAS-CONF-2016-094
30 August 2016

1 Introduction

The ATLAS experiment at the Large Hadron Collider has carried out a large number of searches for beyond the Standard Model (BSM) physics covering a broad range of different final state particles and kinematics. However one gap in the search coverage, as pointed out in Refs. [1, 2], is in final states with one or more lepton, many jets and no-or-little missing transverse momentum (whose magnitude is denoted as $E_{\mathrm{T}}^{\mathrm{miss}}$). Such a search is presented in this note, concentrating on final states with an isolated lepton (electron or muon), large jet multiplicities and either zero or many (three or more) b-tagged jets and with no requirement on $E_{\mathrm{T}}^{\mathrm{miss}}$.

This search has potential sensitivity to a large number of BSM physics models. In this note two R-parity violating (RPV) supersymmetric (SUSY [3–8]) benchmark models are used to interpret the results. In addition, model independent limits on the possible contribution of BSM physics to the signal region yields are presented. The dominant Standard Model (SM) background arises from top-quark pair production and W+jets production. The precise theoretical modelling of these backgrounds at high jet multiplicity suffers from large uncertainties, hence they are estimated from the data by extrapolating the b-tagged jet multiplicity template extracted at moderate jet multiplicities to the high jet multiplicities of the search region.

2 The ATLAS detector

The ATLAS detector [9] is a multi-purpose detector with a forward-backward symmetric cylindrical geometry and nearly 4π coverage in solid angle[1]. The inner tracking detector (ID) consists of pixel and silicon microstrip detectors covering the pseudorapidity region $|\eta| < 2.5$, surrounded by a transition radiation tracker which improves electron identification over the region $|\eta| < 2.0$. The innermost pixel layer, the insertable B-layer [10], was added between Run 1 and Run 2 of the LHC, at a radius of 33 mm around a new, narrower and thinner, beam pipe. The ID is surrounded by a thin superconducting solenoid providing an axial 2 T magnetic field and by a fine-granularity lead/liquid-argon (LAr) electromagnetic calorimeter covering $|\eta| < 3.2$. A steel/scintillator-tile calorimeter provides hadronic coverage in the central pseudorapidity range ($|\eta| < 1.7$). The endcap and forward regions ($1.5 < |\eta| < 4.9$) of the hadronic calorimeter are made of LAr active layers with either copper or tungsten as the absorber material. The muon spectrometer with an air-core toroid magnet system surrounds the calorimeters. Three layers of high-precision tracking chambers provide coverage in the range $|\eta| < 2.7$, while dedicated chambers allow triggering in the region $|\eta| < 2.4$.

The ATLAS trigger system [11, 12] consists of two levels; the first level is a hardware-based system, while the second is a software-based system called the High-Level Trigger.

[1] ATLAS uses a right-handed coordinate system with its origin at the nominal interaction point in the centre of the detector. The positive x-axis is defined by the direction from the interaction point to the centre of the LHC ring, with the positive y-axis pointing upwards, while the beam direction defines the z-axis. Cylindrical coordinates (r, ϕ) are used in the transverse plane, ϕ being the azimuthal angle around the z-axis. The pseudorapidity η is defined in terms of the polar angle θ by $\eta = -\ln\tan(\theta/2)$. The transverse momentum p_{T}, is defined in the x–y plane unless stated otherwise. Rapidity is defined as $y = 0.5\ln\left[(E + p_z)/(E - p_z)\right]$ where E denotes the energy and p_z is the component of the momentum along the beam direction.

3 Data and Simulated Samples

After applying beam, detector and data-quality criteria the data sample analyzed is comprised of 14.8 fb^{-1} of $\sqrt{s}$ = 13 TeV proton–proton (pp) collision data (3.2 fb^{-1} collected in 2015 and 11.6 fb^{-1} collected up to July 15$^{\text{th}}$ 2016) with a minimum pp bunch spacing of 25 ns. In this dataset the mean number of additional pp interactions per proton-bunch crossing (pile-up) is $\langle\mu\rangle$ = 21.4. The luminosity and its uncertainty of ±2.9% are derived following a methodology similar to that detailed in Ref. [13] from a preliminary calibration of the luminosity scale using a pair of x–y beam separation scans performed in August 2015 and June 2016.

Events are recorded online using a single electron or muon trigger with thresholds that give constant efficiency for the event selection used. For the determination of the multi-jet background lepton triggers with less stringent lepton isolation requirements are used as discussed in Section 6. Single photon and multi-jet triggers are also used to select validation samples for the background estimation technique.

Samples of Monte Carlo (MC) simulated events are used to model the signal and for validating the background estimation procedure. In addition, simulated events are used to model the sub-dominant background processes. The response of the detector to particles is modelled with a full ATLAS detector simulation [14] based on GEANT4 [15], or a fast simulation based on a parameterization of the performance of the ATLAS electromagnetic and hadronic calorimeters [16] and on GEANT4 elsewhere. All simulated events are overlaid with pile-up collisions simulated with the soft QCD processes of PYTHIA 8.186 [17] using the A2 set of tunable parameters (tune) [18] and the MSTW2008LO [19] parton distribution function (PDF) set. The simulated events are reconstructed in the same way as the data, and are reweighted so that the distribution of the expected number of collisions per bunch crossing matches the data.

Simulated signal events from two simplified SUSY benchmark models are used to optimize the analysis selections and to estimate the expected signal yields for different signal mass hypotheses. Diagrams of the benchmark signal models are shown in Figure 1. The first model involves pair production of gluinos each of which decays promptly via an off-shell top squark to two top quarks and the lightest neutralino ($\tilde{\chi}_1^0$). The $\tilde{\chi}_1^0$ then decays promptly to three light quarks ($\tilde{\chi}_1^0 \to uds$) via the RPV coupling λ''_{112} with all other RPV couplings set to zero. Samples for this signal model are produced using the HERWIG++ 2.7.1 [20] generator with the CTEQ6L1 [21] PDF set, and using the UEEE5 tune.

The second model involves pair production of gluinos each of which decay promptly to a top quark and a top squark, with the top squark decaying promptly to an s- and a b- quark via a non-zero λ''_{323} RPV coupling. For this model the MG5_aMC@NLO v2.3.3 [22] generator interfaced to PYTHIA 8.210 is used. They are produced with one additional parton in the matrix element and using the A14 [23] tune. Parton luminosities are provided by the NNPDF23LO [24] PDF set.

Signal cross-sections are calculated to next-to-leading order in the strong coupling constant, adding the resummation of soft gluon emission at next-to-leading-logarithmic accuracy (NLO+NLL) [25–29]. The nominal cross-section and the uncertainty are taken from an envelope of cross-section predictions using different PDF sets and factorisation and renormalisation scales, as described in Ref. [30].

The dominant top-quark pair production and W/Z+jets production backgrounds are estimated from the data as described in Section 6, but the expected yields for minor backgrounds are taken from Monte Carlo simulation. In addition, the background estimation procedure is validated with simulated events, and some of the systematic uncertainties are estimated using simulated samples. The samples used are shown in Table 1 and more details on the generator configurations can be found in Refs. [31–34].

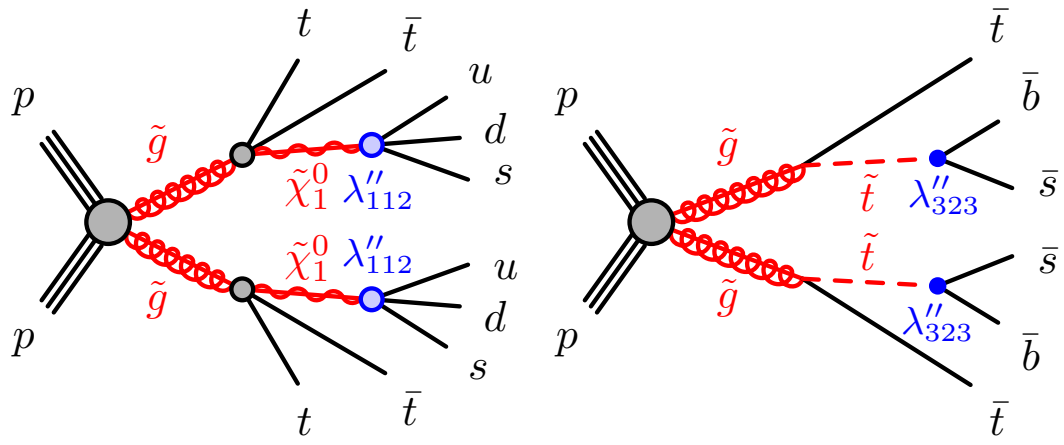

Figure 1: Diagrams of the signal benchmark models. Both models involve pair production of gluinos with each gluino decaying as a) $\tilde{g} \to t\bar{t}\tilde{\chi}_1^0 \to t\bar{t}uds$ b) $\tilde{g} \to \bar{t}\tilde{t} \to \bar{t}\bar{b}\bar{s}$. In both signal scenarios, anti-squarks decay into the charge-conjugate final states of those indicated for the corresponding squarks, and each gluino decays with equal probabilities into the given final state or its charge conjugate.

Physics process	Generator	Parton shower	Cross-section normalisation	PDF set	Tune
$W(\to \ell\nu)$ + jets	Sherpa 2.1.1 [35]	Sherpa 2.1.1	NNLO [36]	NLO CT10 [37]	Sherpa default
$Z/\gamma^*(\to \ell\ell)$ + jets	Sherpa 2.1.1	Sherpa 2.1.1	NNLO [36]	NLO CT10	Sherpa default
$t\bar{t}$	powheg-box v2 [38]	Pythia 6.428 [39]	NNLO+NNLL [40–45]	NLO CT10	Perugia2012 [46]
Single-top (t-channel)	powheg-box v1	Pythia 6.428	NNLO+NNLL [47]	NLO CT10f4	Perugia2012
Single-top (s- and Wt-channel)	powheg-box v2	Pythia 6.428	NNLO+NNLL [48, 49]	NLO CT10	Perugia2012
$t\bar{t}+W/Z/WW$	MG5_aMC@NLO 2.2.2	Pythia 8.186	NLO [22]	NNPDF2.3LO	A14
WW, WZ and ZZ	Sherpa 2.1.1	Sherpa 2.1.1	NLO	NLO CT10	Sherpa default
$t\bar{t}H$	MG5_aMC@NLO	Pythia 8.186	NLO [50]	NNPDF2.3LO	A14

Table 1: Simulated background event samples: the corresponding generator, parton shower, cross-section normalisation, PDF set and underlying-event tune are shown.

4 Object reconstruction and event selection

The reconstructed primary vertex of the event is required to be consistent with the luminous region and to have at least two associated tracks with $p_{\mathrm{T}} > 400$ MeV. The vertex with the largest $\sum p_{\mathrm{T}}^2$ of the associated tracks is chosen as the primary vertex of the event.

Jet candidates are reconstructed using the anti-k_t jet clustering algorithm [51, 52] with jet radius parameter of 0.4 starting from energy clusters of calorimeter cells [53]. The jets are corrected for energy deposits from pile-up collisions using the method suggested in Ref. [54]: a contribution equal to the product of the jet area and the median energy density of the event is subtracted from the jet energy [55]. Further corrections derived from MC simulation and data are used to calibrate on average the energies of jets to the scale of their constituent particles [56]. In the search two jet p_{T} thresholds are used, $p_{\mathrm{T}} > 40$ GeV and $p_{\mathrm{T}} > 60$ GeV, and all jets are required to be within $|\eta| < 2.4$. To minimize the contribution

from jets arising from pile-up interactions, the selected jets must satisfy a loose jet vertex tagger (JVT) requirement [57], where JVT is a quantity that uses tracking and primary vertex information to determine if a given jet originates from the primary vertex. The chosen working point has an efficiency of 94% at a jet p_{T} of 40 GeV and is nearly fully efficient above 60 GeV for true hard-scatter jets. This selection reduces to a negligible level the number of jets originating from, or heavily contaminated by, pile-up interactions. Events with jets originating from detector noise and non-collision background are rejected if the jets fail to satisfy the 'LooseBad' quality criteria, described in Ref. [58].

A multivariate algorithm using information about the impact parameters of inner detector tracks matched to the jet, the presence of displaced secondary vertices, and the reconstructed flight paths of b- and c-hadrons inside the jet [59], is used to identify jets containing a b-hadron (b-jets). The operating point used corresponds to an efficiency of 80% in simulated $t\bar{t}$ events, along with a rejection factor of 106 for gluon and light-quark jets and of 6 for charm jets [60].

Since there is no requirement on $E_{\mathrm{T}}^{\mathrm{miss}}$ or the transverse mass[2], the search is particularly sensitive to fake or non-prompt leptons in multi-jet events. In order to suppress this background to an acceptable level stringent lepton identification and isolation requirements are used.

Muon candidates are formed by combining information from the muon spectrometer and inner tracking detectors and must satisfy the "Medium" quality criteria as described in Ref. [61]. They are required to have $p_{\mathrm{T}} > 35$ GeV and $|\eta| < 2.4$. Furthermore they must satisfy requirements on the significance of the transverse impact parameter with respect to the primary vertex, $|d_0^{\mathrm{PV}}|/\sigma(d_0^{\mathrm{PV}}) < 3$, the longitudinal impact parameter with respect to the primary vertex $|z_0^{\mathrm{PV}}\sin(\theta)| < 0.5$ mm, and the 'Gradient' isolation requirements described in Ref. [61] which rely on the use of tracking-based and calorimeter-based variables and implement a set of η- and p_{T}-dependent criteria.

Electron candidates are reconstructed from an isolated electromagnetic calorimeter energy deposit matched to an ID track and are required to have $p_{\mathrm{T}} > 35$ GeV, $|\eta| < 2.47$, and to satisfy the 'Tight' likelihood-based identification criteria described in Ref. [62]. Electron candidates that fall in the transition region between the barrel and end-cap calorimeter (with $1.37 < |\eta| < 1.52$) are rejected. They are also required to have $|d_0^{\mathrm{PV}}|/\sigma(d_0^{\mathrm{PV}}) < 5$, $|z_0^{\mathrm{PV}}\sin(\theta)| < 0.5$ mm, and to satisfy similar isolation requirements to those applied to muon candidates.

Ambiguities between candidate jets (with $p_{\mathrm{T}} > 20$ GeV) and baseline leptons[3] are resolved as follows: first, any non-b-tagged jet candidate[4] lying within a distance $\Delta R \equiv \sqrt{(\Delta y)^2 + (\Delta\phi)^2} = 0.2$ of a baseline electron is discarded. Furthermore, non-b-tagged jets within $\Delta R = 0.4$ from baseline muons are removed if the number of tracks associated with the jet is less than three or where the ratio of the muon to jet p_{T} is greater than 0.5. Finally, any baseline lepton candidate remaining within a distance $\Delta R = 0.4$ of any surviving jet candidate is discarded.

Corrections derived from data control samples are applied to account for differences between data and simulation for the lepton trigger, reconstruction, identification and isolation efficiencies, the lepton momentum/energy scale and resolution, and for the efficiency and mis-tag rate of the b-tagging algorithm.

[2] The transverse mass between the lepton and the $E_{\mathrm{T}}^{\mathrm{miss}}$ is defined as: $m_{\mathrm{T}}^2 = 2p_T^{\ell}E_{\mathrm{T}}^{\mathrm{miss}}(1 - \cos(\Delta\phi(\ell, E_{\mathrm{T}}^{\mathrm{miss}})))$

[3] Baseline leptons are reconstructed as described above, but with a looser p_{T} requirement ($p_{\mathrm{T}} > 10$ GeV), no isolation or impact parameter requirements, and, in the case of electrons, the "Loose" lepton identification criteria.

[4] In this case a b-tagging working point corresponding to an efficiency of identifying b-jets in a simulated $t\bar{t}$ sample of 85% is used.

5 Analysis Strategy

Events are selected online using a single electron or muon trigger. For the analysis selection at least one electron or muon is required in the event. The analysis is carried out with two sets of jet p_{T} cuts to provide sensitivity to a broader range of possible signals. These cuts are applied to all jets in the event and are $p_{\mathrm{T}} > 40$ GeV, or $p_{\mathrm{T}} > 60$ GeV. The analysis requires at least five jets above the threshold. Events are categorized in two dimensions using the jet multiplicity and the b-tagged jet multiplicity. There are six bins for jet multiplicity (exclusive bins from five to nine jets with an additional ten-or-more jet bin) and five bins for b-tagged jet multiplicity (exclusive bins from zero to three with an additional inclusive four-or-more bin). In this note, the notation $N_{j,b}^{\text{process}}$ is used to denote the number of events predicted by the background fit model, with j jets and b b-tagged jets for a given process, e.g. $N_{j,b}^{t\bar{t}\text{+jets}}$ for $t\bar{t}$+jets events. The number of events summed over all b-tag multiplicity bins for a given number of jets is denoted by N_{j}^{process}, and is also referred to as a jet-slice.

For probing a specific BSM model all of these bins in data are simultaneously fit to constrain the model, in what is labeled a "model-dependent" fit. In the search for an unknown BSM signal, dedicated signal regions (SRs) are defined which could be populated by a possible signal, and where the SM contribution is expected to be small. The expected background in these SRs is estimated from a fit where some of the bins are excluded to limit the effect of signal contamination biasing the background estimate; this setup is labeled a "model-independent" fit. More details on the SR definitions are given in Section 6.5.

The estimation of the dominant background processes of $t\bar{t}$+jets and W/Z+jets production is carried out using a combined fit to the jet and b-tagged jet multiplicity bins described above. The general strategy is to extract a baseline template of the b-tag multiplicity distribution in events with five jets and to parameterize the dependence of the template on the number of jets based on the observed evolution in events with larger jet multiplicities. The assumptions used in the parameterization are validated using data and MC simulation. Furthermore, the background determination assumes that there is no significant signal contribution to events with five or six jets.

6 Background estimation

6.1 W/Z+jets

A partially data-driven approach is used to estimate the W/Z+jets background. While the shape of the b-tag multiplicity spectra are taken from simulated events, the normalization is derived from the data. The estimate of the normalization relies on the assumption that the probability of additional jet radiation is constant, for events above a certain minimum number of jets [63–65]. This leads to a simple scaling behaviour [66] between the number of W/Z+jets events with n and $n+1$ jets, that has been observed by the ATLAS [67, 68] and CMS [69] Collaborations.

The scaling ratio r is defined as $r = N_{j+1}^{W/Z\text{+jets}}/N_{j}^{W/Z\text{+jets}}$. The number of W/Z+jets events with different jet multiplicities is then parameterized as follows:

$$N_{j,b}^{W/Z\text{+jets}} = \frac{\mathrm{MC}_{j,b}^{W/Z\text{+jets}}}{\mathrm{MC}_{j}^{W/Z\text{+jets}}} \cdot k^{W/Z\text{+jets}} \cdot \mathrm{MC}_{5}^{W/Z\text{+jets}} \cdot r^{(j-5)}, \tag{1}$$

where $\mathrm{MC}_{j,b}^{W/Z+\mathrm{jets}}$ and $\mathrm{MC}_{j}^{W/Z+\mathrm{jets}}$ are the predicted numbers of W/Z + j jets events with b b-tags and inclusive in b-tags, respectively, both taken from MC simulation, and $k^{W/Z+\mathrm{jets}}$ is the absolute normalization in five jet events expressed relative to the predicted number of events from MC simulation. The term $k^{W/Z+\mathrm{jets}} \cdot \mathrm{MC}_{5}^{W/Z+\mathrm{jets}} \cdot r^{(j-5)}$ gives the number of b-tag inclusive events in the j jet slice, and the ratio $\mathrm{MC}_{j,b}^{W/Z+\mathrm{jets}}/\mathrm{MC}_{j}^{W/Z+\mathrm{jets}}$ is the fraction of b b-tagged events in this jet slice. The parameters $k^{W/Z+\mathrm{jets}}$ and r are left freely floating in the fit and are therefore extracted from the data along with the other background contributions.

Due to different b-tagged jet multiplicity spectra in W+jets and Z+jets events, the two processes are treated separately. They are normalized in control regions with five or six jets and zero b-tags. For the Z+jets normalization, the control regions are defined selecting events with two oppositely charged same flavour leptons fulfilling an invariant mass requirement around the Z boson mass ($81 \leq m_{\ell\ell} \leq 101$ GeV), as well as the requirement of exactly five or exactly six jets, and zero b-tags. The W+jets normalization relies on control regions containing the remaining events with exactly five or exactly six jets, and zero b-tags, which, for each jet multiplicity, is split by the electric charge of the leading (with the highest p_{T}) lepton. The expected charge asymmetry in W+jets events is taken from MC simulation separately for five jet and six jet events and used to constrain the normalization from the data using these control regions. Although all parameters are determined in a global likelihood fit, the dominant constraining power on the absolute normalization comes from the five-jet control regions, and the dominant constraints on the r parameter originate from the combination of the five-jet and six-jet control regions. The contamination of $t\bar{t}$ events in the two lepton control regions is negligible, whereas in the control regions used to estimate the W+jets normalization it is significant and is discussed in Section 6.2. Once the two processes are normalized they are scaled using the same common scaling factor r. While independent scaling factors could be used, tests in data show that no significant difference is present and therefore a common parameter is used.

The assumption of constant jet scaling is validated in data using γ+jets and multi-jet events, and also W+jets and Z+jets MC samples are found to be consistent with this assumption. The γ+jets events are selected using a photon trigger, and an isolated photon [70] with $p_{\mathrm{T}} > 145$ GeV is required in the event selection, whereas the multi-jet events are selected using unprescaled multi-jet triggers, where the trigger thresholds only allow jets with $p_{\mathrm{T}} > 50$ GeV to be probed down to seven jets, and $p_{\mathrm{T}} > 60$ GeV to six jets. In both cases selections are applied to ensure these control regions probe similar kinematic phase-space to that relevant for the analysis. Figure 2 shows the jet multiplicity distribution for these processes for different jet p_{T} thresholds, showing good compatibility with the assumption of an exponentially falling distribution.

6.2 $t\bar{t}$+jets

A data-driven model is used to estimate the number of events from $t\bar{t}$+jets production in a given jet and b-tag multiplicity bin. The basic concept of this model is based on the extraction of an initial template of the b-tag multiplicity spectrum in events with five jets and the parameterization of the evolution of this template to higher jet multiplicities. The absolute normalization is determined independently in each jet multiplicity slice. The extrapolation of the b-tag multiplicity spectrum to higher jet multiplicities starts from the assumption that the difference in the b-tag multiplicity spectrum in events with n and $n+1$ jets arises mainly from the production of additional jets, and can be described by a fixed probability that the additional jet is b-tagged. Given the small mistag rate this probability is dominated by the probability that the additional jet is a heavy-flavour jet which is b-tagged. In order to account for acceptance effects

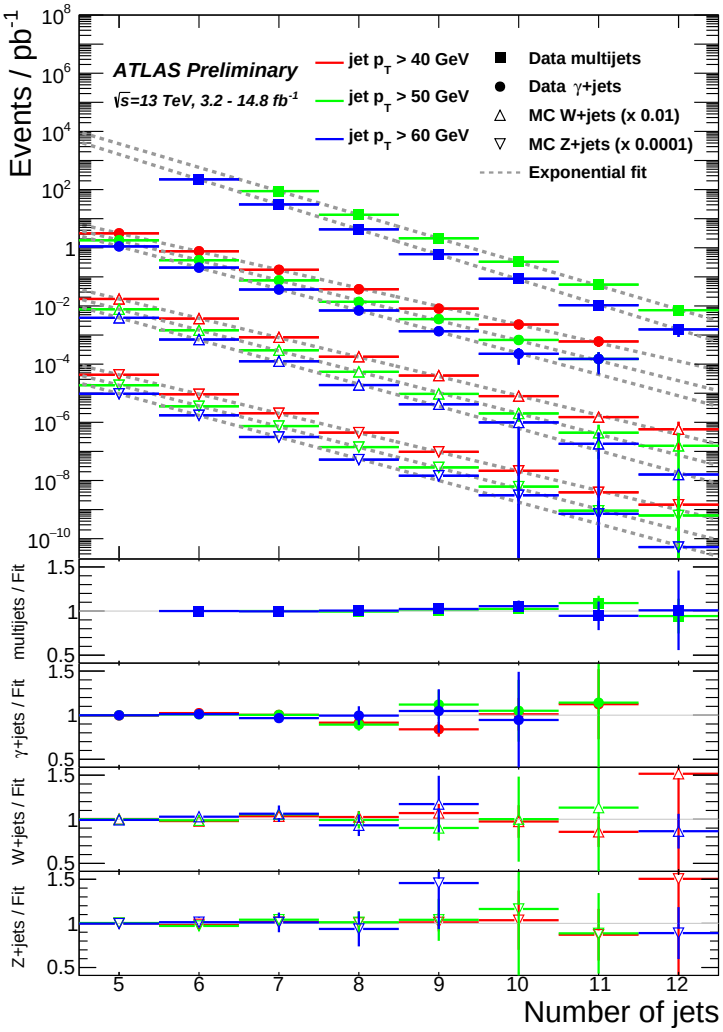

Figure 2: The expected jet multiplicity distribution in W+jets and Z+jets MC simulation, as well as the distribution from γ+jet and multi-jet data control regions, for jet p_{T} thresholds of 40 GeV, 50 GeV and 60 GeV (note the trigger thresholds do not allow the 40 GeV threshold nor the low jet multiplicities to be studied in the multi-jet events). In each case the distribution is fitted with an exponential function. The bottom panels show the ratio of the points to the fit function separately for each process.

due to the different kinematics in events with high jet-multiplicity, the probability of further b-tagged jets entering into acceptance is also taken into account. The extrapolation over one additional jet can be parameterized as:

$$\begin{aligned} N_{j,b}^{t\bar{t}+\mathrm{jets}} &= N_{j}^{t\bar{t}+\mathrm{jets}} \cdot f_{j,b} \\ f_{(j+1),b} &= f_{j,b} \cdot x_0 + f_{j,(b-1)} \cdot x_1 + f_{j,(b-2)} \cdot x_2 \end{aligned} \tag{2}$$

where $N_{j}^{t\bar{t}+\mathrm{jets}}$ is the number of $t\bar{t}$+jets events with j jets, which is determined independently in each jet multiplicity slice, and $f_{j,b}$ is the fraction of $t\bar{t}$ events with j jets of which b are b-tagged. The parameters x_i describe the probability of one additional jet to be either not b-tagged (x_0), b-tagged (x_1) or b-tagged and leading to a second b-tagged jet to move into the fiducial acceptance (x_2). The latter is dominated

by cases where the extra jet is a b-jet and it influences the kinematics of the event such that an additional b-jet, that was below the jet p_{T} threshold, enters into the acceptance. Given that the x_i parameters describe probabilities, the sum $\sum_i x_i = 1$ is normalized to unity. Subsequent application of this parameterization produces a b-tag template for arbitrarily high jet-multiplicities.

Studies based on MC simulated events corresponding to very large equivalent luminosities as well as studies using fully efficient truth-level b-tagging, suggested the addition of a fit parameter that allows for correlated production of two b-tagged jets[5] (as may be expected with b-jet production from gluon splitting). It was found that this effect is sufficiently small after the fiducial acceptance cuts to be ignored in this phenomenological model for the given integrated luminosity.

The initial b-tag multiplicity template is extracted from data events with five jets after subtracting all other background processes, and is denoted as i_b and scaled by the absolute normalization $N_5^{t\bar{t}+\text{jets}}$ in order to obtain the model in the five jet bin:

$$N_{5,b}^{t\bar{t}+\text{jets}} = N_5^{t\bar{t}+\text{jets}} \cdot i_b = N_5^{t\bar{t}+\text{jets}} \cdot f_{5,b} \tag{3}$$

where the sum $\sum_{b=0}^{\geq 4} i_b = 1$, is normalized to unity.

Since the last jet multiplicity bin is inclusive in the number of jets, a correction is applied to correct the jet-exclusive estimate described above to a jet-inclusive estimate (referred to as the *exclusive-to-inclusive correction*). As the jet multiplicity spectrum falls approximately exponentially the correction is small ($\leq$ 10%) and is taken from simulation.

The model described above is based on the assumption that any change of the b-tag multiplicity spectrum is due to additional jet radiation with a certain probability to lead to b-tagged jets. There is, however, also a small increase in the acceptance for b-jets produced in the decay of the $t\bar{t}$ system when increasing the jet multiplicity due to the on average higher jet momentum. The effect amounts to up to 5% in the one and two b-tag bins for high jet multiplicities, and is taken into account using a correction to the initial template extracted from simulated $t\bar{t}$ events.

The zero b-tag component of the initial $t\bar{t}$ template which is extracted from events with five jets exhibits a strong anti-correlation with the absolute W+jets normalization which is extracted in the same bin. The control regions separated in leading lepton charge detailed in Section 6.1 provide a handle to extract the absolute W+jets normalization, however as this is a somewhat weak constraint there remains an anti-correlation that does not affect the total background estimate. For these control regions the $t\bar{t}$+jets process is assumed to be charge symmetric and the model is simply split into two halves for these bins.

6.3 Multi-jet events

The contribution from multi-jet production with a fake or non-prompt (FNP) lepton (such as hadrons mis-identified as leptons, leptons originating from heavy-flavour decays, and electrons from photon conversions), constitutes a minor but non-negligible background, especially in the lower jet multiplicity slices. It is estimated from the data with a matrix method similar to that described in Ref. [71]. In this method, two types of lepton identification criteria are defined: "tight", corresponding to the default lepton criteria described in Section 4, and "loose", corresponding to baseline leptons after overlap removal. The

[5] This is implemented by changing the evolution described in equation 2 such that any term with $x_1 \cdot x_1$ is replaced by $x_1 \cdot x_1 \cdot \rho_{11}$, where ρ_{11} describes the correlated production of two b-tagged jets.

matrix method relates the number of events containing prompt or FNP leptons to the number of observed events with tight or loose-not-tight leptons using the probability for loose-prompt or loose-FNP leptons to satisfy the tight criteria. The probability for loose prompt leptons to satisfy the tight selection criteria is obtained using a $Z \to \ell\ell$ data sample and is modelled as a function of the lepton p_{T}. The probability for loose FNP leptons to satisfy the tight selection criteria is determined from a data control region enriched in non-prompt leptons with a loose-lepton, multiple jets, low-$E_{\mathrm{T}}^{\mathrm{miss}}$ [72, 73] and low transverse mass. The efficiencies are measured as a function of p_{T} after subtracting the contribution from prompt lepton processes and are assumed to be independent of the jet multiplicity[6].

6.4 Small backgrounds

The small background contribution from diboson production, single top production and $t\bar{t}$ production in association with a vector/Higgs boson (labeled $t\bar{t}V/H$) are estimated using MC simulated event samples. The sum of these backgrounds contribute not more than ≈10% of the SM expectation in any of the jet and b-tag multiplicity bins.

6.5 Fit configuration and validation

The search results are determined from a simultaneous likelihood fit. The likelihood is built as the product of a Poisson probability density function describing the observed numbers of events in the different bins and Gaussian distributions constraining the nuisance parameters associated with the systematic uncertainties whose widths correspond to the sizes of these uncertainties. Poisson distributions are used instead for MC and data control region statistical uncertainties. Correlations of a given nuisance parameter between the different sources of backgrounds and the signal are taken into account when relevant.

The likelihood is configured slightly differently for the "model-dependent", and for the "model-independent" hypothesis tests. The former is used to derive exclusion limits for a specific BSM model, and the full set of bins (5 to 10 inclusive and $b = 0$ to 4 inclusive) is employed in the likelihood. The signal contribution, as predicted by the given BSM model, is considered in all bins and scaled by one common signal strength parameter. The number of freely floating parameters of the background model is 15. Three in the W/Z+jets model: the jet scaling parameter (r), and the normalization of the W+jets and Z+jets events in the five jet region ($k^{W+\mathrm{jets}}$ and $k^{Z+\mathrm{jets}}$). In addition there are 12 parameters in the $t\bar{t}$+jets background model: six for the overall normalizations of the different jet-slices ($N_j^{t\bar{t}+\mathrm{jets}}$, $j = 5-10$), four for the initial b-tag multiplicity template (i_b, $b = 1-4$), and two for the evolution parameters (x_1, x_2), taking into account the constraints: $x_0 = 1 - x_1 - x_2$, and $i_0 = 1 - \sum_{b=1}^{\geq 4} i_b$. The number of fitted bins[7] is 34, leading to an over-constrained system.

The model-independent test is used to search for, and to set generic exclusion limits on, the potential contribution of an unknown BSM signal in the phase-space probed by this analysis. For this purpose dedicated signal regions are defined which could be populated by such a possible signal, and where the SM contribution is expected to be small. For each jet p_{T} threshold these signal regions are defined in terms of jet and b-tag multiplicity requirements as shown in Table 2. Due to the efficiency of the b-tagging

[6] To minimise the dependence on the number of jets, the event selection considers only the leading baseline lepton when checking the more stringent identification and isolation criteria of the "tight" lepton definitions.

[7] Five b-tag bins in the seven-to-ten jet slices, and seven bins (the zero b-tag bin is split into three bins for each of the W/Z CRs) in the five and six jet slices.

algorithm used, signal models with large b-tag multiplicities can have significant contamination in the two b-tag bin which can bias the $t\bar{t}$+jets background estimate reducing the sensitivity of the search. To avoid this effect, for the ≥ 3 b-tag SRs, the two b-tag bin is not included in the fit for the high jet multiplicity slices; the exact bins that are excluded from the fit for each SR are shown in Table 2. Even excluding the two b-tag bins, signal contamination in the one b-tag bin can weaken the sensitivity, as the signal contribution can be absorbed into the $t\bar{t}$+jets normalization.

Jet requirement	b-tag jet requirement	Bins excluded from fit to avoid signal contamination
≥ 8	$= 0$	≥ 8 jet 0 b-tag
≥ 8	≥ 3	≥ 8 jet ≥ 3 b-tag and ≥ 8 jet 2 b-tag
≥ 9	$= 0$	≥ 9 jet 0 b-tag
≥ 9	≥ 3	≥ 9 jet ≥ 3 b-tag and ≥ 9 jet 2 b-tag
≥ 10	$= 0$	≥ 10 jet 0 b-tag
≥ 10	≥ 3	≥ 10 jet ≥ 3 b-tag and ≥ 10 jet 2 b-tag

Table 2: Definition of the model-independent signal regions used. Each signal region is studied with a 40 GeV and a 60 GeV jet p_{T} threshold. The last column lists the jet-multiplicity / b-tag multiplicity bins not included in the fit to estimate the background for that SR.

For the "model-independent" hypothesis tests, a separate likelihood fit is performed for each SR. A potential signal contribution is considered in the given SR bin only. The number of freely floating parameters of the background model is between 13 (for the SRs with $j \geq 8$) and 15 (for the SRs with $j \geq 10$) due to the number of $t\bar{t}$ normalizations parameters. The number of observables varies between 21 ($j \geq 8$ and $b \geq 3$) and 33 ($j \geq 10$ and $b = 0$), hence the system is also always over-constrained.

The fit setup has been extensively tested using MC simulated events, and has been demonstrated to give a negligible bias in the fitted yields, both in the case where the background only distributions are fit, or when a signal is injected into the fitted data. In addition when fitting the data the fitted parameter values and their inter-correlations were studied in detail and found to be in agreement with the expectation based on MC simulated event samples. The estimate of the multi-jet background has been validated in data regions enriched in FNP leptons, and been found to describe the data within the quoted uncertainties.

7 Systematic Uncertainties

The dominant backgrounds are estimated from the data without the use of MC simulation, and therefore the main systematic uncertainties related to the estimation of these backgrounds arise from the assumptions made in the W/Z+jets, $t\bar{t}$+jets and multi-jet background estimates. Uncertainties related to the theoretical modelling of the specific processes and due to the modelling of the detector response in simulated events are only relevant for the minor backgrounds (diboson, single top-quark and $t\bar{t}V/H$ which are taken from MC simulation) and for the estimates of the signal yields after selections.

For the W/Z+jets background estimation, the uncertainty related to the assumed scaling behaviour is taken from studies of this behaviour in W+jets, Z+jets MC simulation, as well as in γ+jets and multi-jet data control regions chosen to be kinematically similar to the search selection (see Figure 2). No evidence is seen for a violation of the assumed scaling behaviour and the statistical precision of these methods is used as an uncertainty (up to 18% for the highest jet multiplicity bins). The expected uncertainty

on the charge-asymmetry for W+jets production is $\approx$ 3% from PDF variations, but in the five and six jet regions, where this constraint is applied, the uncertainty due to the limited number of MC events is considerably larger (10-20% depending on the jet p_{T} threshold applied). The uncertainty on the shape of the b-tag multiplicity distribution in W+jets and Z+jets events is derived by comparing different MC generator setups (e.g. varying the renormalisation and factorisation scale and the parton-shower). It is seen to grow as a function of jet multiplicity and is $\approx$ 50% for events with five jets after which the MC statistical uncertainty becomes very large. An uncertainty of 100% is therefore assigned on the fractional contribution from W+b and W+c events for all jet multiplicity slices considered, which has a very small impact on the final result.

The uncertainties related to the $t\bar{t}$+jets background estimation primarily relate to the number of events in the data regions used for the fit. As mentioned in Section 6.2 the method shows good closure using simulated event samples, and adding more flexibility to the fit does not affect the results, so no systematic uncertainty related to these studies is assigned. There is a small uncertainty related to the acceptance correction of the initial b-tag multiplicity template, which is derived by varying the MC generator setup for the $t\bar{t}$ sample used to estimate the correction. This leads to a 3% uncertainty on the correction and has no significant effect on the final uncertainty. In addition a 100% uncertainty is assigned on the exclusive-to-inclusive correction (which is defined in Section 6.2 and is derived from MC simulation) for the highest jet multiplicity bins used.

The dominant uncertainties on the multi-jet background estimate arise from the number of data events in the control regions, uncertainties related to the subtraction of electroweak backgrounds from these control regions (here a 20% uncertainty is applied on the expected yield of the backgrounds in the control regions) and uncertainties to cover the possible dependencies of the real- and fake- efficiencies on variables other than lepton p_{T} (for example the dependence on the number of jets in the event). The total uncertainty on the multi-jet background is $\approx$ 50%.

The uncertainty on the expected yields of the minor backgrounds include theoretical uncertainties on the cross-sections and on the modelling of the kinematics by the MC generator, as well as experimental uncertainties related to the modelling of the detector response in the simulation. The uncertainties assigned to cover the theoretical estimate of these backgrounds in the relevant regions are 50%, 100% and 30% for diboson, single top-quark, $t\bar{t}V$, and $t\bar{t}H$ productions, respectively. An additional uncertainty, related to the theoretical modelling of additional b-jets arising from initial or final state radiation in the simulated samples is assigned by comparing the $t\bar{t}$+jets estimate in high b-tag regions with the prediction from $t\bar{t}$ simulation. Since the additional b-jets are mostly coming from the parton-shower which is similar for the different MC samples, this is used as a systematic uncertainty. The dominant experimental uncertainties relate to the modelling of the jet energy scale, the jet energy resolution, and the b-tagging efficiencies and mis-tagging rates.

The systematic uncertainties related to the background estimation do not play a big role in the final uncertainty on the background estimates in the SRs apart from the sizeable uncertainty on the expected charge-asymmetry of W+jets production. Reducing this statistically limited uncertainty in the future will improve the precision of the W+jets estimate.

The uncertainties assigned on the expected signal yield for the SUSY benchmark processes considered include the experimental uncertainties related to the detector modelling, which are dominated by the modelling of the jet energy scale, the jet energy resolution, and the b-tagging efficiencies and mis-tagging rates. The uncertainty on the signal cross-sections used is discussed in Section 3.

8 Results

Results are provided both as model-independent limits on the contribution from BSM physics to the dedicated signal regions and in the context of the two SUSY benchmark models discussed in Section 3. As previously mentioned, different fit setups are used for these two sets of results. In all cases the profile-likelihood-ratio test [74] is used to establish 95% confidence intervals using the CL_s prescription [75].

Figures 3 and 4 show the observed numbers of data events compared to the fitted background model, for the two jet p_T thresholds respectively. The likelihood fit is configured using the model-dependent setup where all bins are input to the fit, and fixing the signal strength parameter to zero. An example signal model is also shown to illustrate the separation between the signal and the background achieved, as well as the level of the leakage of the signal events into lower b-tag and jet multiplicity bins. The bottom panel of each figure shows the background prediction using MC simulation, which indicate for high b-tag multiplicities (≥ 3) a strong underprediction by the MC simulation compared to the data-driven background estimation. This effect has been observed before [76, 77] and shows that the MC simulations are not able to correctly describe high b-jet multiplicity final states.

8.1 Model independent results

The model-independent results are calculated from the observed number of events, and the expected background in the SRs, where in each case the background has been estimated using a fit that excludes the bins shown in Table 2 in order to limit the bias on the background estimation introduced by a signal. Table 3 shows the expected background in the SRs from these fits together with the observed numbers of events for the sets of SRs with the 40 GeV and 60 GeV jet p_T thresholds. In addition, the p_0 values are shown, which quantify the probability that a background-only experiment results in a fluctuation equal or larger than the one observed in the data. The largest deviation is observed in the (0 b-tag, ≥ 9 jet) bin for $p_T^{\text{jet}} > 60$ GeV corresponding to a 2.3σ excess.

Model-independent upper limits at 95% confidence level (CL) on the number of BSM events, N_{BSM}, that may contribute to the signal regions are computed from the fits. Normalizing these results by the integrated luminosity L of the data sample, they can be interpreted as upper limits on the visible BSM cross-section σ_{vis}, defined as the product $\sigma_{\text{prod}} \times A \times \epsilon = N_{\text{BSM}}/L$ of production cross-section (σ_{prod}), acceptance (A) and reconstruction efficiency (ϵ). These limits are presented in Table 4.

For a possible unknown signal with ≈ 4 b-jets the analysis sensitivity is reduced due to the possible leakage of signal events into lower b-tag jet multiplicities due to the value of the b-tagging efficiency, which would bias the normalization of the $t\bar{t}$+jets background. This is partially mitigated by not using the two b-tag bins in the background determination for the highest jet multiplicities probed. In order to check further that the data does not resemble a signal, the $t\bar{t}$+jets normalization, fitted as a free parameter in each jet multiplicity slice, is examined in Figure 5 for the data and for the $t\bar{t}$+jets MC simulation, for both the 40 GeV and 60 GeV jet p_T thresholds. The effect of adding signal events onto the $t\bar{t}$+jets simulation is also shown. The $t\bar{t}$+jets normalization fitted from the data as a function of the jet multiplicity is consistent with the expected distribution from $t\bar{t}$+jets MC simulation.

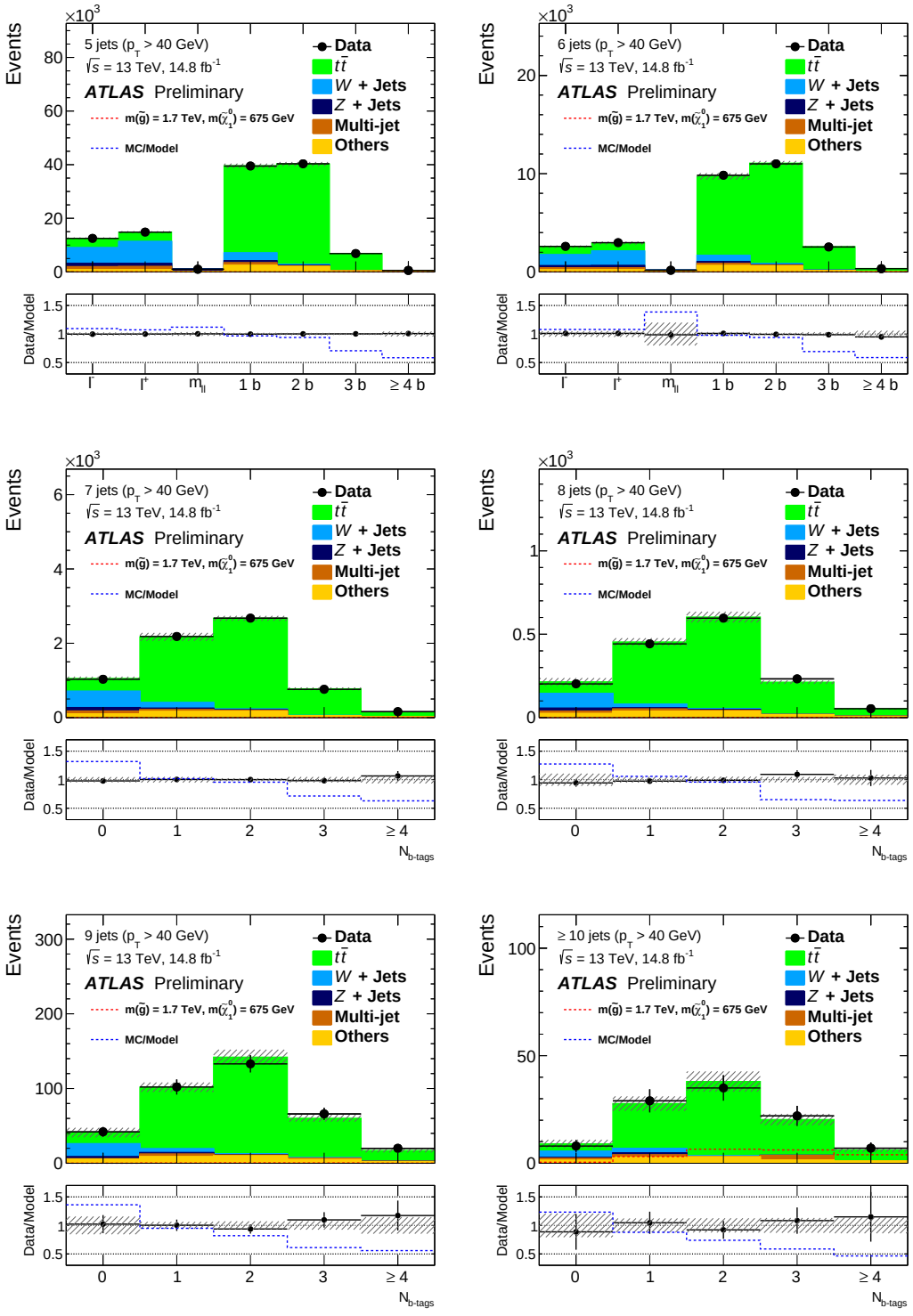

Figure 3: The expected background and observed data in the different jet and b-tag multiplicity bins for the 40 GeV jet p_{T} threshold. The background shown is estimated by including all bins in the fit. For the five and six jet slices the control regions used to estimate the W+jets and Z+jets normalization are also shown (labeled ℓ^-, ℓ^+, and $m_{\ell\ell}$). An example signal for the $\tilde{g} \to t\bar{t}\tilde{\chi}_1^0 \to t\bar{t}uds$ model with $m_{\tilde{g}}$ = 1700 GeV and $m_{\tilde{\chi}_1^0}$ = 675 GeV is also shown (although its contribution is very small with this jet p_{T} threshold). The bottom panels show the ratio between the observed data and the background prediction, as well as the ratio between the estimated background and the prediction from MC simulation. All uncertainties are included in the error bands (shaded regions), which are correlated between bins.

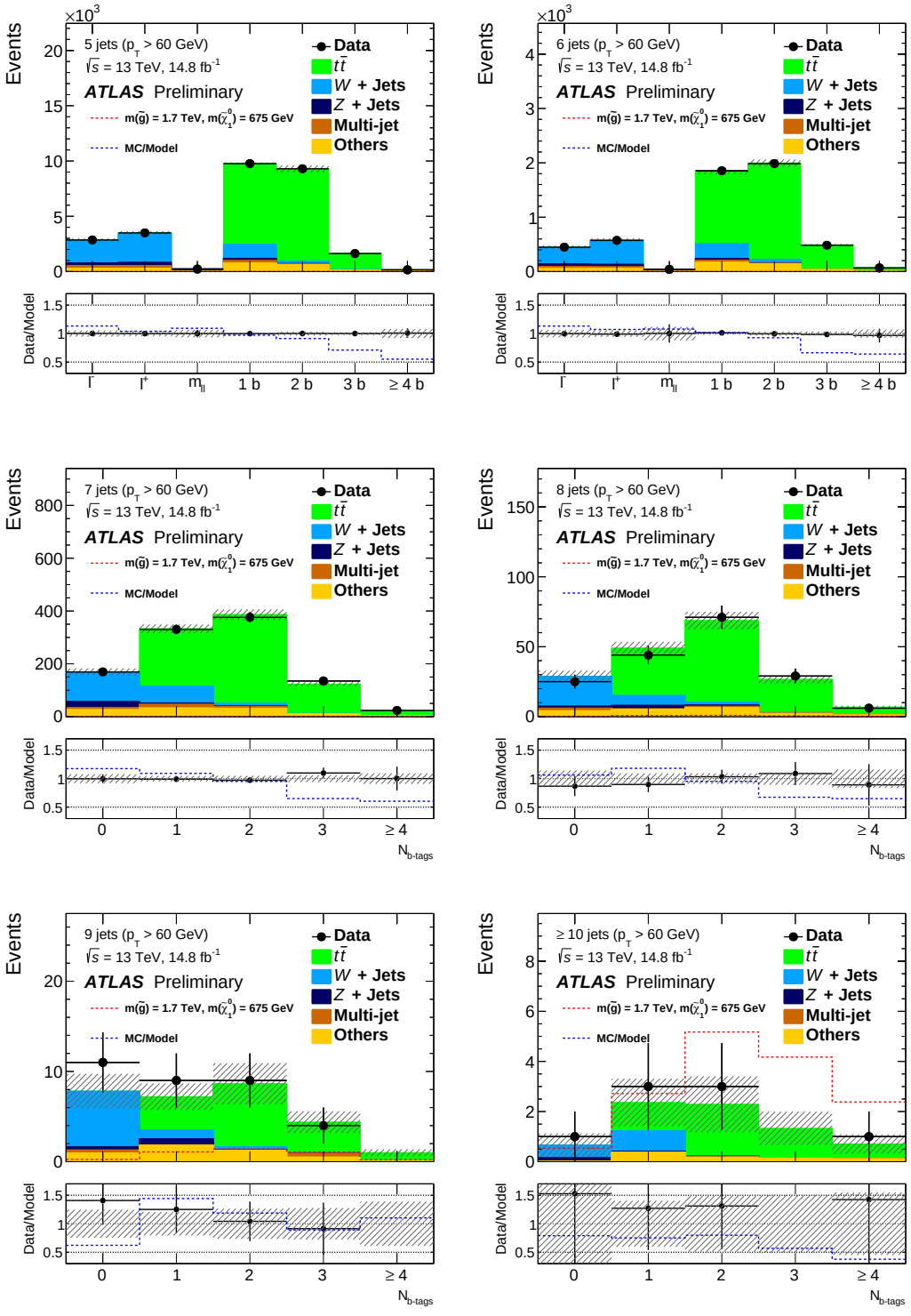

Figure 4: The expected background and observed data in the different jet and b-tag multiplicity bins for the 60 GeV jet p_{T} threshold. The background shown is estimated by including all bins in the fit. For the five and six jet slices the control regions used to estimate the W+jets and Z+jets normalization are also shown (labeled ℓ^-, ℓ^+, and $m_{\ell\ell}$). An example signal for the $\tilde{g} \to t\bar{t}\tilde{\chi}_1^0 \to t\bar{t}uds$ model with $m_{\tilde{g}}$ = 1700 GeV and $m_{\tilde{\chi}_1^0}$ = 675 GeV is also shown (although its contribution is very small in most of the jet multiplicity slices shown). The bottom panels show the ratio between the observed data and the background prediction, as well as the ratio between the estimated background and the prediction from MC simulation. All uncertainties are included in the error bands (shaded regions), which are correlated between bins.

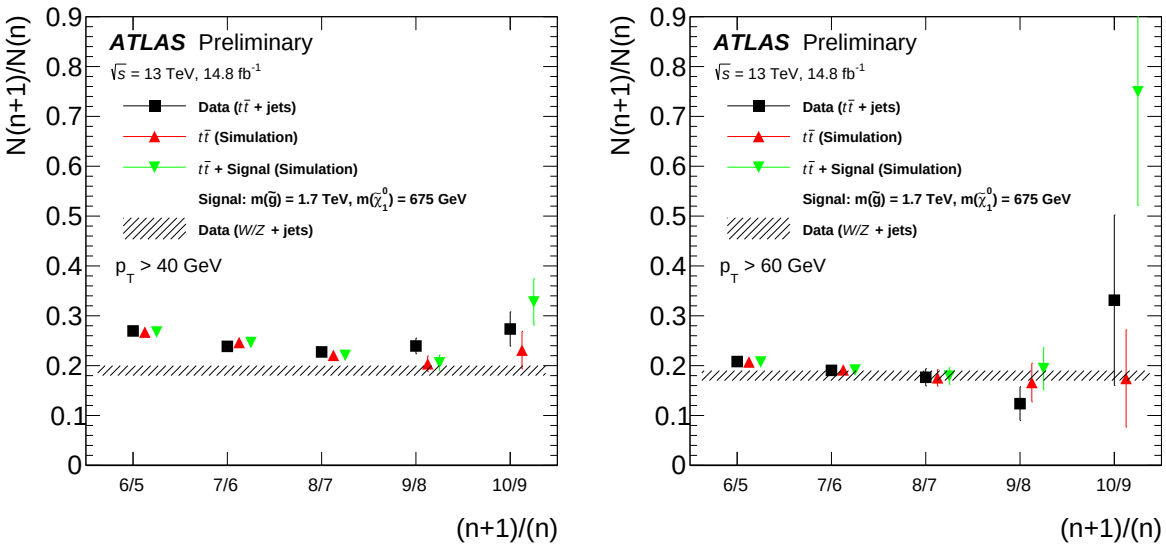

Figure 5: The scaling behaviour of the fitted number of $t\bar{t}$ +jets events as a function of the jet multiplicity for jet p_{T} thresholds of 40 GeV (left) and 60 GeV (right) for both data and $t\bar{t}$+jets simulation. The normalization parameters are extracted from a combined background model fit to data or simulated events. The effect of injecting a benchmark signal for the $\tilde{g} \to t\bar{t}\tilde{\chi}_1^0 \to t\bar{t}uds$ model with $m_{\tilde{g}} = 1700$ GeV and $m_{\tilde{\chi}_1^0} = 675$ GeV onto the $t\bar{t}$+jets simulation is also shown. Also shown as a hashed band is the scaling behaviour for W/Z+jets events fitted from the data as part of the background model fit. The uncertainties between bins are correlated.

8.2 Model dependent results

For each signal model probed, the fit is configured using the model-dependent setup, as detailed in Section 6.5. All bins are included in the fit and the expected signal contribution in each bin is taken into account. Figure 6 shows the observed and expected exclusion limits in the two considered benchmark signal models, as a function of the gluino and neutralino or top squark masses. Since the background prediction from MC simulation does not reflect the expected background contribution, the expected limit is computed using the background prediction from a fit to all bins in the data with no signal component in the fit model.

In the model with an RPV decay of the $\tilde{\chi}_1^0$ to three light-quark jets, gluino masses up to 1750 GeV are excluded, with slightly weaker limits for light and heavy $\tilde{\chi}_1^0$. In the benchmark model with $\tilde{g} \to t\bar{t}\tilde{t}$ and $\tilde{t} \to \bar{b}\bar{s}$, gluino masses up to 1400 GeV are excluded. For both benchmark models all the probed model points have the best expected sensitivity using the 60 GeV jet p_{T} threshold selection, and so that is used to set the exclusion limits.

The acceptance times efficiency ($A \times \epsilon$) for the $\tilde{g} \to t\bar{t}\tilde{\chi}_1^0 \to t\bar{t}uds$ model for the ≥ 10 jet, ≥ 3 b-tag SR with the 60 GeV jet p_{T} threshold is typically $\approx 8\%$, whereas for the $\tilde{g} \to t\bar{t}\tilde{t} \to t\bar{t}\bar{b}\bar{s}$ model for the ≥ 8 jet, ≥ 3 b-tag SR with the 60 GeV jet p_{T} threshold it is typically $\approx 4\%$.

9 Conclusion

A search for beyond the Standard Model physics in events with an isolated lepton (electron or muon), high jet multiplicity and no, or many, b-tagged jets is presented. Unlike previous searches, no requirement on $E_{\mathrm{T}}^{\mathrm{miss}}$ is applied. A novel data-driven background estimation technique is used to estimate the dominant background from $t\bar{t}$+jets and W/Z+jets production. The analysis is performed with proton–proton collision data at $\sqrt{s}$ = 13 TeV collected between August 2015 and July 2016 with the ATLAS detector at the Large Hadron Collider corresponding to an integrated luminosity of 14.8 fb^{-1}. With no significant excess over the Standard Model expectation observed, results are interpreted in the framework of simplified models featuring gluino pair production in R-parity violating supersymmetry scenarios. In a benchmark model with $\tilde{g} \to t\bar{t}\tilde{\chi}_1^0 \to t\bar{t}uds$, gluino masses up to 1.75 TeV are excluded at 95% confidence level. In a model with $\tilde{g} \to \bar{t}\tilde{t}$ with $\tilde{t} \to bs$, gluino masses up to 1.4 TeV are excluded. In addition model-independent limits are set on the contribution of new phenomena to the signal region yields of up to 8 fb at 95% confidence level.

Jet p_T > 40 GeV	≥ 8 Jets		≥ 9 Jets		≥ 10 Jets	
Process	0b	≥ 3 b	0b	≥ 3 b	0b	≥ 3 b
$t\bar{t}$+jets	69 ± 35	301 ± 30	19 ± 8	90 ± 12	3.4 ± 1.6	23 ± 6
W+jets	150 ± 50	1.5 ± 1.3	20 ± 7	0.7 ± 0.7	3.3 ± 1.5	< 0.1
Others	30 ± 13	27 ± 12	7 ± 4	8.1 ± 2.9	1.5 ± 0.7	2.4 ± 0.8
Z+jets	22 ± 4	0.61 ± 0.10	3.0 ± 0.8	0.32 ± 0.08	0.47 ± 0.16	< 0.1
Multijet	19 ± 9	3.1 ± 1.3	1.3 ± 0.7	3.3 ± 1.8	0.9 ± 0.5	1.7 ± 0.9
Total Bkd.	286 ± 20	333 ± 29	50 ± 4	102 ± 12	9.6 ± 1.1	27 ± 6
Data	252	400	50	115	8	29
p_0 (σ)	0.5 (0)	0.03 (1.9)	0.5 (0)	0.20 (0.8)	0.5 (0)	0.39 (0.3)
Jet p_T > 60 GeV	≥ 8 Jets		≥ 9 Jets		≥ 10 Jets	
Process	0b	≥ 3 b	0b	≥ 3 b	0b	≥ 3 b
$t\bar{t}$+jets	4 ± 4	32 ± 8	0.4 ± 0.6	10 ± 6	< 0.1	3.1 ± 3.1
W+jets	22 ± 7	0.33 ± 0.32	3.2 ± 1.6	0.11 ± 0.11	0.41 ± 0.26	< 0.1
Others	5.0 ± 2.3	4.2 ± 1.6	0.75 ± 0.30	1.1 ± 0.4	< 0.1	0.30 ± 0.09
Z+jets	1.7 ± 0.4	< 0.1	0.29 ± 0.08	< 0.1	0.110 ± 0.035	< 0.1
Multijet	2.1 ± 1.1	1.2 ± 0.6	0.15 ± 0.08	0.43 ± 0.22	0.0	0.0
Total Bkd.	34 ± 5	38 ± 8	4.7 ± 1.3	12 ± 6	0.55 ± 0.28	3.4 ± 3.1
Data	37	40	12	5	1	1
p_0 (σ)	0.35 (0.4)	0.41 (0.2)	0.01 (2.3)	0.5 (0)	0.31 (0.5)	0.5 (0)

Table 3: The observed data and fitted background yields in the signal regions. The parameters of the model are determined in fits to reduced sets of bins as discussed in the text. The individual background uncertainties can be substantially larger than the total uncertainty due to correlations between parameters. The p_0 values (and associated σ values) represent the probabilities (significances in units of standard deviations) that the observed numbers of events are compatible with the background-only hypothesis. The values are set to 0.5 (σ = 0) if the number of observed events is smaller or equal to the background yield.

Jet multiplicity	0b obs. [fb]	0b exp. [fb]	$\geq$ 3b obs. [fb]	$\geq$ 3b exp. [fb]
$\geq$ 8 jets (p_{T} > 40 GeV)	2.2	$3.3^{+1.3}_{-0.9}$	8.4	$4.7^{+2.0}_{-1.3}$
$\geq$ 9 jets (p_{T} > 40 GeV)	1.1	$1.1^{+0.5}_{-0.3}$	2.8	$2.1^{+0.9}_{-0.6}$
$\geq$ 10 jets (p_{T} > 40 GeV)	0.43	$0.52^{+0.26}_{-0.14}$	1.19	$1.1^{+0.45}_{-0.31}$
$\geq$ 8 jets (p_{T} > 60 GeV)	1.2	$1.1^{+0.4}_{-0.3}$	1.5	$1.4^{+0.5}_{-0.4}$
$\geq$ 9 jets (p_{T} > 60 GeV)	0.97	$0.46^{+0.22}_{-0.13}$	0.5	$0.6^{+0.2}_{-0.2}$
$\geq$ 10 jets (p_{T} > 60 GeV)	0.2	$0.2^{+0.1}_{-0.1}$	0.26	$0.29^{+0.14}_{-0.08}$

Table 4: Observed and expected 95% CL model-independent upper limits on the product of cross-section, acceptance and efficiency (in fb) for each signal region. The limits are determined fitting the background model in a reduced set of bins as described in the text.

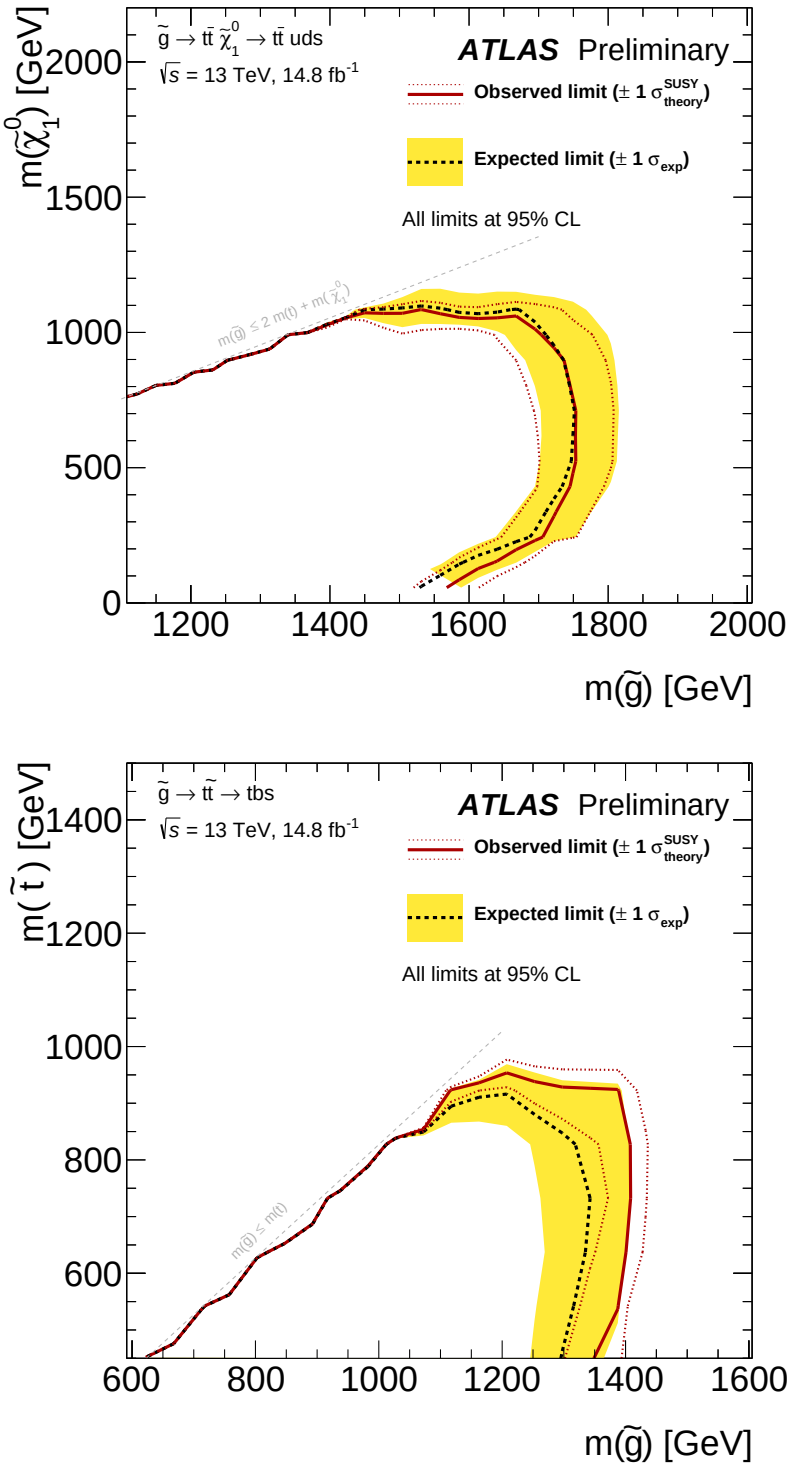

Figure 6: Observed and expected exclusion limits on the $\tilde{g}$ and $\tilde{\chi}_1^0$ or $\tilde{t}$ masses in the context of the RPV SUSY scenarios probed, with simplified mass spectra featuring $\tilde{g}\tilde{g}$ pair production with exclusive decay modes. The contours of the band around the expected limit are the $\pm 1\sigma$ results, including all uncertainties except theoretical uncertainties on the signal cross-section. The dotted lines around the observed limit illustrate the change in the observed limit as the nominal signal cross-section is scaled up and down by the theoretical uncertainty. All limits are computed at 95% CL. The diagonal lines indicate the kinematic limit for the decays in each specified scenario.

References

[1] M. Lisanti et al., *Study of LHC Searches for a Lepton and Many Jets*, JHEP **11** (2012) 081, arXiv: 1107.5055 [hep-ph].

[2] J. A. Evans et al., *Toward Full LHC Coverage of Natural Supersymmetry*, JHEP **07** (2014) 101, arXiv: 1310.5758 [hep-ph].

[3] Yu. A. Golfand and E. P. Likhtman, *Extension of the Algebra of Poincare Group Generators and Violation of p Invariance*, JETP Lett. **13** (1971) 323, [Pisma Zh. Eksp. Teor. Fiz.13,452(1971)].

[4] D. V. Volkov and V. P. Akulov, *Is the Neutrino a Goldstone Particle?*, Phys. Lett. B **46** (1973) 109.

[5] J. Wess and B. Zumino, *Supergauge Transformations in Four-Dimensions*, Nucl. Phys. B **70** (1974) 39.

[6] J. Wess and B. Zumino, *Supergauge Invariant Extension of Quantum Electrodynamics*, Nucl. Phys. B **78** (1974) 1.

[7] S. Ferrara and B. Zumino, *Supergauge Invariant Yang-Mills Theories*, Nucl. Phys. B **79** (1974) 413.

[8] A. Salam and J. A. Strathdee, *Supersymmetry and Nonabelian Gauges*, Phys. Lett. B **51** (1974) 353.

[9] ATLAS Collaboration, *The ATLAS Experiment at the CERN Large Hadron Collider*, JINST **3** (2008) S08003.

[10] ATLAS Collaboration, *ATLAS Insertable B-Layer Technical report Design Report*, ATLAS-TDR-19 (2010), URL: http://cds.cern.ch/record/1291633.

[11] ATLAS Collaboration, *Performance of the ATLAS Trigger System in 2010*, Eur. Phys. J. C **72** (2012) 1849, arXiv: 1110.1530 [hep-ex].

[12] The ATLAS TDAQ Collaboration, *The ATLAS Data Acquisition and High Level Trigger system*, JINST **11** (2016) P06008.

[13] ATLAS Collaboration, *Improved luminosity determination in pp collisions at $\sqrt{s}$ = 7 TeV using the ATLAS detector at the LHC*, Eur. Phys. J. C **73** (2013) 2518, arXiv: 1302.4393 [hep-ex].

[14] ATLAS Collaboration, *The ATLAS Simulation Infrastructure*, Eur.Phys.J. **C70** (2010) 823, arXiv: 1005.4568 [physics.ins-det].

[15] S. Agostinelli et al., *GEANT4: A Simulation toolkit*, Nucl.Instrum.Meth. **A506** (2003) 250.

[16] ATLAS Collaboration, *The simulation principle and performance of the ATLAS fast calorimeter simulation FastCaloSim*, ATL-PHYS-PUB-2010-013, 2010, URL: http://cds.cern.ch/record/1300517.

[17] T. Sjöstrand, S. Mrenna and P. Z. Skands, *A Brief Introduction to PYTHIA 8.1*, Comput.Phys.Commun. **178** (2008) 852, arXiv: 0710.3820 [hep-ph].

[18] ATLAS Collaboration, *Further ATLAS tunes of Pythia 6 and Pythia 8*, ATL-PHYS-PUB-2011-014, 2011, URL: http://cds.cern.ch/record/1400677.

[19] A. Sherstnev and R. Thorne, *Parton Distributions for LO Generators*, Eur.Phys.J. **C55** (2008) 553, arXiv: 0711.2473 [hep-ph].

[20] G. Corcella et al., *HERWIG 6: An Event generator for hadron emission reactions with interfering gluons (including supersymmetric processes)*, JHEP **0101** (2001) 010, arXiv: hep-ph/0011363 [hep-ph].

[21] J. Pumplin et al., *New generation of parton distributions with uncertainties from global QCD analysis*, JHEP **07** (2002) 012, arXiv: hep-ph/0201195 [hep-ph].

[22] J. Alwall et al., *The automated computation of tree-level and next-to-leading order differential cross sections, and their matching to parton shower simulations*, JHEP **07** (2014) 079, arXiv: 1405.0301 [hep-ph].

[23] ATLAS Collaboration, *ATLAS Pythia 8 tunes to 7 TeV data*, ATL-PHYS-PUB-2014-021, 2014, URL: http://cdsweb.cern.ch/record/1966419.

[24] R. D. Ball et al., *Parton distributions with LHC data*, Nucl. Phys. **B867** (2013) 244, arXiv: 1207.1303 [hep-ph].

[25] W. Beenakker et al., *Squark and gluino production at hadron colliders*, Nucl.Phys. **B492** (1997) 51, arXiv: hep-ph/9610490 [hep-ph].

[26] A. Kulesza and L. Motyka, *Threshold resummation for squark-antisquark and gluino-pair production at the LHC*, Phys.Rev.Lett. **102** (2009) 111802, arXiv: 0807.2405 [hep-ph].

[27] A. Kulesza and L. Motyka, *Soft gluon resummation for the production of gluino-gluino and squark-antisquark pairs at the LHC*, Phys.Rev. **D80** (2009) 095004, arXiv: 0905.4749 [hep-ph].

[28] W. Beenakker et al., *Soft-gluon resummation for squark and gluino hadroproduction*, JHEP **0912** (2009) 041, arXiv: 0909.4418 [hep-ph].

[29] W. Beenakker et al., *Squark and gluino hadroproduction*, Int.J.Mod.Phys. **A26** (2011) 2637, arXiv: 1105.1110 [hep-ph].

[30] M. Kramer et al., *Supersymmetry production cross sections in pp collisions at* $\sqrt{s} = 7$ *TeV*, (2012), arXiv: 1206.2892 [hep-ph].

[31] ATLAS Collaboration, *Simulation of top-quark production for the ATLAS experiment at* $\sqrt{s} = 13$ *TeV*, ATL-PHYS-PUB-2016-004, 2016, URL: http://cdsweb.cern.ch/record/2120417.

[32] ATLAS Collaboration, *Monte Carlo Generators for the Production of a W or* Z/γ^* *Boson in Association with Jets at ATLAS in Run 2*, ATL-PHYS-PUB-2016-003, 2016, URL: http://cdsweb.cern.ch/record/2120133.

[33] ATLAS Collaboration, *Multi-boson simulation for 13 TeV ATLAS analyses*, ATL-PHYS-PUB-2016-002, 2016, URL: http://cdsweb.cern.ch/record/2119986.

[34] ATLAS Collaboration, *Modelling of the* $t\bar{t}H$ *and* $t\bar{t}V$ $(V = W, Z)$ *processes for* $\sqrt{s} = 13$ *TeV ATLAS analyses*, ATL-PHYS-PUB-2016-005, 2016, URL: https://cds.cern.ch/record/2120826.

[35] T. Gleisberg et al., *Event generation with SHERPA 1.1*, JHEP **02** (2009) 007, arXiv: 0811.4622 [hep-ph].

[36] S. Catani et al.,
Vector boson production at hadron colliders: a fully exclusive QCD calculation at NNLO,
Phys. Rev. Lett. **103** (2009) 082001, arXiv: 0903.2120 [hep-ph].

[37] H.-L. Lai et al., *New parton distributions for collider physics*, Phys. Rev. D **82** (2010) 074024, arXiv: 1007.2241 [hep-ph].

[38] S. Alioli et al., *A general framework for implementing NLO calculations in shower Monte Carlo programs: the POWHEG BOX*, JHEP **1006** (2010) 043, arXiv: 1002.2581 [hep-ph].

[39] T. Sjöstrand, S. Mrenna and P. Z. Skands, *PYTHIA 6.4 Physics and Manual*, JHEP **05** (2006) 026, arXiv: hep-ph/0603175.

[40] M. Czakon, P. Fiedler and A. Mitov,
Total Top-Quark Pair-Production Cross Section at Hadron Colliders Through $O(\alpha_S^4)$,
Phys. Rev. Lett. **110** (2013) 252004, arXiv: 1303.6254 [hep-ph].

[41] M. Czakon and A. Mitov,
NNLO corrections to top pair production at hadron colliders: the quark-gluon reaction,
JHEP **1301** (2013) 080, arXiv: 1210.6832 [hep-ph].

[42] M. Czakon and A. Mitov, *NNLO corrections to top-pair production at hadron colliders: the all-fermionic scattering channels*, JHEP **1212** (2012) 054, arXiv: 1207.0236 [hep-ph].

[43] P. Bärnreuther, M. Czakon and A. Mitov, *Percent Level Precision Physics at the Tevatron: First Genuine NNLO QCD Corrections to $q\bar{q} \to t\bar{t} + X$*, Phys. Rev. Lett. **109** (2012) 132001, arXiv: 1204.5201 [hep-ph].

[44] M. Cacciari et al., *Top-pair production at hadron colliders with next-to-next-to-leading logarithmic soft-gluon resummation*, Phys. Lett. B **710** (2012) 612, arXiv: 1111.5869 [hep-ph].

[45] M. Czakon and A. Mitov,
Top++: A Program for the Calculation of the Top-Pair Cross-Section at Hadron Colliders,
Comput. Phys. Commun. **185** (2014) 2930, arXiv: 1112.5675 [hep-ph].

[46] P. Z. Skands, *Tuning Monte Carlo Generators: The Perugia Tunes*,
Phys. Rev. D **82** (2010) 074018, arXiv: 1005.3457 [hep-ph].

[47] N. Kidonakis, *Next-to-next-to-leading-order collinear and soft gluon corrections for t-channel single top quark production*, Phys. Rev. D **83** (2011) 091503, arXiv: 1103.2792 [hep-ph].

[48] N. Kidonakis,
Two-loop soft anomalous dimensions for single top quark associated production with a W- or H-,
Phys. Rev. D **82** (2010) 054018, arXiv: 1005.4451 [hep-ph].

[49] N. Kidonakis, *NNLL resummation for s-channel single top quark production*,
Phys. Rev. D **81** (2010) 054028, arXiv: 1001.5034 [hep-ph].

[50] S. Dittmaier et al., *Handbook of LHC Higgs Cross Sections: 1. Inclusive Observables*, (2011), arXiv: 1101.0593 [hep-ph].

[51] M. Cacciari, G. P. Salam and G. Soyez, *The anti-k_t jet clustering algorithm*, JHEP **04** (2008) 063, arXiv: 0802.1189 [hep-ph].

[52] M. Cacciari and G. P. Salam, *Dispelling the N^3 myth for the k_t jet-finder*,
Phys. Lett. B **641** (2006) 57, arXiv: hep-ph/0512210.

[53] ATLAS Collaboration,
Topological cell clustering in the ATLAS calorimeters and its performance in LHC Run 1, (2016), arXiv: 1603.02934 [hep-ex].

[54] M. Cacciari and G. P. Salam, *Pileup subtraction using jet areas*, Phys. Lett. B **659** (2008) 119, arXiv: 0707.1378 [hep-ph].

[55] ATLAS Collaboration, *Pile-up subtraction and suppression for jets in ATLAS*, ATLAS-CONF-2013-083, 2013, URL: http://cdsweb.cern.ch/record/1570994.

[56] ATLAS Collaboration, *Jet Calibration and Systematic Uncertainties for Jets Reconstructed in the ATLAS Detector at* $\sqrt{s}$ = 13 *TeV*, ATL-PHYS-PUB-2015-015, 2015, URL: https://cds.cern.ch/record/2037613.

[57] ATLAS Collaboration, *Tagging and suppression of pileup jets with the ATLAS detector*, ATLAS-CONF-2014-018, 2014, URL: http://cdsweb.cern.ch/record/1700870.

[58] ATLAS Collaboration,
Selection of jets produced in 13 *TeV proton–proton collisions with the ATLAS detector*, ATLAS-CONF-2015-029, 2015, URL: http://cdsweb.cern.ch/record/2037702.

[59] ATLAS Collaboration, *Performance of b-Jet Identification in the ATLAS Experiment*, JINST **11** (2016) P04008, arXiv: 1512.01094 [hep-ex].

[60] ATLAS Collaboration, *Optimisation of the ATLAS b-tagging performance for the 2016 LHC Run*, 2016, URL: http://cds.cern.ch/record/2160731.

[61] ATLAS Collaboration, *Muon reconstruction performance of the ATLAS detector in proton–proton collision data at* $\sqrt{s}$ *=13 TeV*, (2016), arXiv: 1603.05598 [hep-ex].

[62] ATLAS Collaboration,
Electron identification measurements in ATLAS using $\sqrt{s}$ = 13 *TeV data with* 50 *ns bunch spacing*, ATL-PHYS-PUB-2015-041, 2015, URL: http://cdsweb.cern.ch/record/2048202.

[63] S. Ellis, R. Kleiss and W. Stirling, *W's, Z's and jets*, Physics Letters B **154** (1985) 435, URL: http://www.sciencedirect.com/science/article/pii/0370269385904253.

[64] F. Berends et al., *Multijet production in W, Z events at pp colliders*, Physics Letters B **224** (1989) 237, URL: http://www.sciencedirect.com/science/article/pii/0370269389910812.

[65] W. Giele and W. Stirling, *Top search at fermilab: Multijet signals and backgrounds*, Nuclear Physics B **343** (1990) 14, URL: http://www.sciencedirect.com/science/article/pii/0550321390905922.

[66] E. Gerwick et al., *Scaling Patterns for QCD Jets*, JHEP **1210** (2012) 162, arXiv: 1208.3676 [hep-ph].

[67] ATLAS Collaboration, *Measurement of the production cross section of jets in association with a Z boson in pp collisions at* $\sqrt{s}$ = 7 *TeV with the ATLAS detector*, JHEP **07** (2013) 032, arXiv: 1304.7098 [hep-ex].

[68] ATLAS Collaboration, *Measurements of the Production Cross Section of a Z boson in Association with Jets in pp collisions at sqrt(s) = 13TeV with the ATLAS Detector*, ATLAS-CONF-2016-046, 2016, URL: http://cdsweb.cern.ch/record/2206128.

[69] CMS Collaboration,
Jet production rates in association with W and Z bosons in pp collisions at $\sqrt{s} = 7$ *TeV*,
JHEP **2012** (2012) 1, URL: http://dx.doi.org/10.1007/JHEP01(2012)010.

[70] ATLAS Collaboration, *Measurements of the photon identification efficiency with the ATLAS detector using* 4.9 fb^{-1} *of pp collision data collected in 2011*, ATLAS-CONF-2012-123, 2012, URL: http://cdsweb.cern.ch/record/1473426.

[71] ATLAS Collaboration, *Search for supersymmetry at* $\sqrt{s} = 13$ *TeV in final states with jets and two same-sign leptons or three leptons with the ATLAS detector*, Eur. Phys. J. **C76** (2016) 259, arXiv: 1602.09058 [hep-ex].

[72] ATLAS Collaboration, *Performance of missing transverse momentum reconstruction with the ATLAS detector in the first proton–proton collisions at* $\sqrt{s} = 13$ *TeV*, ATL-PHYS-PUB-2015-027, 2015, URL: http://cdsweb.cern.ch/record/2037904.

[73] ATLAS Collaboration, *Expected performance of missing transverse momentum reconstruction for the ATLAS detector at* $\sqrt{s} = 13$ *TeV*, ATL-PHYS-PUB-2015-023, 2015, URL: http://cdsweb.cern.ch/record/2037700.

[74] G. Cowan et al., *Asymptotic formulae for likelihood-based tests of new physics*, Eur. Phys. J. **C71** (2011) 1554, [Erratum: Eur. Phys. J. **C73** (2013) 2501], arXiv: 1007.1727 [physics.data-an].

[75] A. L. Read, *Presentation of search results: the CL s technique*, Journal of Physics G: Nuclear and Particle Physics **28** (2002) 2693.

[76] CMS Collaboration, *Measurement of the cross section ratio* $\sigma_{ttbb}/\sigma_{ttjj}$ *using dilepton final states in pp collisions at sqrt(s) = 13 TeV*, CMS PAS TOP-16-010, 2016, URL: http://cdsweb.cern.ch/record/2202803.

[77] ATLAS Collaboration, *Search for the Standard Model Higgs boson produced in association with top quarks and decaying into* $b\bar{b}$ *in pp collisions at* $\sqrt{s} = 13$ *TeV with the ATLAS detector*, ATLAS-CONF-2016-080, 2016, URL: http://cds.cern.ch/record/2206255.